



HAL
open science

Application of the modified Dubinin-Astakhov equation for a better understanding of high-pressure hydrogen adsorption on activated carbons

Giuseppe Sdanghi, S. Schaefer, G. Maranzana, A. Celzard, V. Fierro

► **To cite this version:**

Giuseppe Sdanghi, S. Schaefer, G. Maranzana, A. Celzard, V. Fierro. Application of the modified Dubinin-Astakhov equation for a better understanding of high-pressure hydrogen adsorption on activated carbons. *International Journal of Hydrogen Energy*, 2019, 45 (48), pp.25912-25926. 10.1016/j.ijhydene.2019.09.240 . hal-02357721

HAL Id: hal-02357721

<https://hal.science/hal-02357721>

Submitted on 10 Nov 2019

HAL is a multi-disciplinary open access archive for the deposit and dissemination of scientific research documents, whether they are published or not. The documents may come from teaching and research institutions in France or abroad, or from public or private research centers.

L'archive ouverte pluridisciplinaire **HAL**, est destinée au dépôt et à la diffusion de documents scientifiques de niveau recherche, publiés ou non, émanant des établissements d'enseignement et de recherche français ou étrangers, des laboratoires publics ou privés.

Application of the modified Dubinin-Astakhov equation for a better understanding of high- pressure hydrogen adsorption on activated carbons

G. Sdanghi^{1,2}, S. Schaefer¹, G. Maranzana², A. Celzard¹, V. Fierro^{1*}

¹ Institut Jean Lamour, UMR CNRS-Université de Lorraine n°7198, ENSTIB, 27 rue
Philippe Seguin, BP 21042, F-88051 EPINAL Cedex 9, France

² Laboratoire d'Energétique et de Mécanique Théorique et Appliquée, UMR CNRS-
Université de Lorraine n°7563, 2 avenue de la Forêt de Haye, BP 160, F-54504
Vandœuvre-lès-Nancy, France

* Corresponding author. Tel: + 33 372 74 96 77. Fax: + 33 372 74 96 38. E-mail address :
Vanessa.Fierro@univ-lorraine.fr (V. Fierro)

Abstract

Hydrogen storage in activated carbons (ACs) has proven to be a realistic alternative to compression and liquefaction. Adsorption capacities up to 5.8 wt.% have indeed been obtained. The amount of adsorbed hydrogen depends on the textural properties of ACs, such as specific surface area and total pore volume. The modified Dubinin-Astakhov (MDA) equation proved to be a good analytical tool for describing hydrogen adsorption in a wide range of pressures and temperatures and for several adsorbents. The parameters of this model have been found to be somehow related to the textural properties of the adsorbent. Thus, we applied this model to understand better hydrogen adsorption on ACs over a wide range of pressures in relation to the textural properties of the ACs.

We applied the MDA equation to evaluate also the isosteric heat of hydrogen adsorption, which was found to be in the range of 5 to 9 kJ mol⁻¹. We compared the results obtained by applying the MDA equation with those obtained by both the sorption isosteric method and the Sips equation. This allowed finding the temperature dependence of the isosteric heat of adsorption, as well as its variation with respect to the textural properties of the ACs.

1. Introduction

The increase in both global warming and worldwide energy demand requires a transition to divestment of fossil fuels and the use of clean and environmentally friendly sources of energy [1–5]. Hydrogen could be a valid alternative to fossil fuels [6–9], but its low volumetric energy density ($0.01079 \text{ MJ L}^{-1}$ STP, much lower than that of gasoline, 34 MJ L^{-1}) hinders the development of adequate and safe storage systems. Among all the methods nowadays adopted for hydrogen storage [10], physisorption on activated carbons (ACs) is quite promising [11] because no chemical bond between hydrogen and the carbon surface is involved, thus giving completely reversible hydrogen uptakes and releases [12,13] with adsorption energies between 4 and 8 kJ mol^{-1} [14].

Hydrogen adsorption on ACs has proven to be a more advantageous way to store hydrogen than pure compression up to 20 MPa at room temperature [15]. To store 5 kg of hydrogen at 20 MPa and at room temperature, a tank with a volume of 340 L would be needed if hydrogen is purely compressed, whereas a volume of 263 L would be necessary under the same conditions if the tank is filled with ACs [16,17]. Further improvements are possible at cryogenic temperatures due to the higher density of the adsorbed phase [18]. At 77 K, the amount of adsorbed hydrogen stored in microporous carbons is predominant relative to the amount of hydrogen in the gas phase, especially at low pressure, and significantly increases the total storage compared to the pure compression under identical temperature and pressure conditions. Thus, the adsorbed phase represents approximately 60% of the maximum storage capacity measured at 2 MPa [19], leading to the possibility of adopting a cryogenic hydrogen adsorption system for storing hydrogen, the efficiency of which would essentially depend on two main features: (i) AC textural properties and (ii) thermal management of the entire system.

With regard to the textural properties of ACs, the physisorption of hydrogen is enhanced on microporous carbons with high specific surface areas [20,21]. The maximum storage capacity and the specific surface area of ACs are related to each other by the “Chahine rule”, which assumes that the hydrogen uptake on ACs increases progressively by 1 wt.% per 500 m² g⁻¹ of specific surface area at 77 K [22]. However, Dubinin [23] stated that in microporous adsorbents, the concept of surface area loses its physical significance because hydrogen uptake is due to pore volume filling and not to monolayer adsorption. Thus, high hydrogen uptakes can be achieved with ACs having substantially high micropore volumes, the optimal micropore diameter depending on pressure and temperature [24].

The hydrogen adsorption capacities on ACs are among the highest ever reached and reported in the open literature [25], regardless of the carbon precursor (i.e., anthracites, bituminous coal or cellulose [26–28]). A hydrogen excess capacity as high as 6.4 wt.% at 77 K and 4 MPa with ACs having a micropore volume of 0.87 cm³ g⁻¹ is among the best results ever obtained for a carbon material [15]. This value is higher than the gravimetric hydrogen storage recommended by the DOE for automotive applications, i.e., 5.5 wt.% by 2025 [29,30]. Nevertheless, not only the weight of the adsorbent but that of the whole system must be taken into account in the DOE target and, therefore, a hydrogen capacity well above 5.5 wt.% should be reached if only the adsorbent is considered. As a result, the DOE target remains difficult to reach at room temperature [31], although hydrogen storage capacities can be improved by doping with metal nanoparticles or heteroatoms [32,33].

Appropriate heat management is necessary to achieve good hydrogen storage performance, as hydrogen adsorption on ACs is an exothermic process [34]. Thus, hydrogen adsorption increases the temperature and significantly affects the net hydrogen storage capacity if the heat of adsorption is not evacuated [35]. Indeed, Hermosilla-Lara et al. [36] found that the heat of adsorption contributes up to 22% of all the thermal effects involved in a cryogenic

adsorption system. Rogacka et al. [37] showed that the heat of adsorption is independent of the gas pressure in the narrow pores, whereas it becomes pressure-dependent as the pore size increases. Moreover, Broom et al. [38] found that the usable capacity of hydrogen in an adsorption system could be increased by reducing the heat of adsorption.

The heat of adsorption is generally evaluated by using the sorption isosteric method [39], which consists in applying the Clausius-Clapeyron equation to the adsorption isotherms calculated over a wide range of temperature and pressures. The latter method reliably determines the isosteric heat of adsorption [40], which ranges from 3 to 7.5 kJ mol⁻¹ [41] for hydrogen adsorption on the Metal Organic Framework (MOF) MIL-101 and on different microporous carbon adsorbents [42]. The smallest pores contribute the most to the average heat of adsorption and are the first to be filled [43], and the heat of adsorption decreases with the surface coverage [44,45].

In the present study, hydrogen adsorption on two commercial ACs with different textural characteristics was investigated in the temperature range of 77 to 273 K and up to 15 MPa. The relationship between textural properties and hydrogen adsorption capacity for the two ACs was analysed by using the Modified Dubinin-Astakhov (MDA) equation, proposed by Richard et al. [46]. The MDA equation was also used to evaluate the isosteric heat of hydrogen adsorption, and the results obtained from this approach were compared to those obtained by using the sorption isosteric method and the Sips model. This approach allowed us to analyse (i) the temperature dependence of the isosteric heat of hydrogen adsorption and (ii) its variation with the textural properties of the selected ACs. These two questions are fundamental for developing and designing efficient hydrogen storage systems by cryo-adsorption.

2. Experimental

2.1 Textural properties of ACs

In this study, two super-activated carbons (ACs) from Kansai Coke & ChemicalsTM (Japan) were selected, the MAXSORB[®] MSC-30 and MSP20X.

The textural characterization of both MSC-30 and MSP20X was performed using a Micromeritics[®] ASAP 2020 automatic adsorption apparatus. The samples were outgassed under vacuum at 523 K until the pressure stabilised around 0.2-0.4 mPa for more than 24 h prior to any adsorption measurement. Both nitrogen adsorption at 77 K and carbon dioxide adsorption at 273 K were carried out. All data was processed using Micromeritics[®] Microactive software.

The surface areas were first calculated with the BET method to compare our results with those reported in the open literature. The BET area, A_{BET} , was then obtained using the BET equation in the range of relative pressures 0.01-0.05, according to Rouquerol [47]. Pore size distributions (PSDs) were obtained by non-local density function theory (NLDFT) using the SAIEUS[®] software of Jagiello et al. [48]. SAIEUS[®] provides more accurate PSDs by combining N₂ and CO₂ adsorption data. By integrating the PSDs over the entire range of pore sizes [49], we also obtained the S_{NLDFT} surface areas. The average micropore diameter, L_0 , was calculated using the NLDFT model. Micropore volumes were evaluated by both the NLDFT model and the Dubinin-Raduskevich (DR) equation. Finally, the NLDFT was also used to calculate the micropore surface areas.

2.2 Hydrogen adsorption measurements

The hydrogen adsorption measurements were carried out in the temperature range of 77 to 273 K and up to 15 MPa using the HPVA II high-pressure volumetric device from

Micromeritics-Particulate Systems. Temperature control was achieved through a one-stage closed-cycle cryogenic refrigerator providing accurate temperature control with an error margin of ± 0.005 K and capable of operating between 25 and 350 K. A sample cell of 10 cm^3 of volume was used for the measurements, filled with an amount of carbon of about 1.2 g. Prior to any measurement, the sample was outgassed under vacuum (6×10^{-4} Pa) at 423 K for 10 h. The pressure steps chosen for hydrogen adsorption were 0.1, 0.5, 0.8, 1, 2, 3, 5, 7.5, 10, 12.5 and 14 MPa, while pressure steps for desorption were 11.5, 8, 4.5, 1.5 and 0.5 MPa. The contribution of the empty cell was systematically measured at each temperature and subtracted.

The isosteric heat of adsorption, Q_{st} , was calculated using the isosteric method [39] from the Micromeritics[®] Microactive 4.01 software, based on the Clausius-Clapeyron equation:

$$-\frac{Q_{st}}{R} = \frac{\partial \ln(P)}{\partial(1/T)} \quad (1)$$

where R is the universal gas constant ($8.314 \text{ J mol}^{-1} \text{ K}^{-1}$), P is the absolute pressure (Pa) and T is the temperature (K). Q_{st} was calculated using nine isotherms at nine different temperatures between 93 and 253 K.

3. Modelling

3.1 Modified Dubinin-Astakhov (MDA) equation

Experimental storage data provide values of excess hydrogen adsorption, n_{exc} [mol/kg], particularly when volumetric methods are used for measurements. It is defined as the difference between the hydrogen uptake on the surface of AC at a specific temperature and pressure and the amount that would be present in the same volume and at the same temperature and pressure in the absence of adsorption forces [13]:

$$n_{exc} = n_{abs} - \rho_g V_a \quad (2)$$

where n_{abs} [mol kg⁻¹] is the absolute amount of adsorbed hydrogen, ρ_g [kg m⁻³] is the hydrogen bulk phase density and V_a [m³ kg⁻¹] is the volume of the adsorbed phase. V_a is considered constant by several authors [46,50,51], thus the adsorbed hydrogen is supposed to occupy a defined volume near the surface of the carbon where the adsorption field exists, and where its density increases gradually up to an asymptotic value. V_a cannot be measured experimentally. According to Eq. (2), excess adsorption isotherms exhibit a maximum. Indeed, ρ_g increases significantly at high pressures, while n_{abs} does not increase anymore once it reaches its maximum value at a specific pressure.

We used the Modified Dubinin-Astakhov (MDA) equation proposed by Richard et al. [46] to model hydrogen excess adsorption on ACs:

$$n_{exc} = n_{max} \exp\left(\left(\frac{RT}{\alpha + \beta T}\right)^2 \ln^2\left(\frac{P_0}{P}\right)\right) - \rho_g V_a \quad (3)$$

The model requires 5 parameters: n_{max} [mol kg⁻¹] is the amount of adsorbed hydrogen corresponding to the saturation of the total available porous volume, α [J mol⁻¹] is an “enthalpy” factor, β [mol J⁻¹ K⁻¹] is an “entropy” factor [52] and P_0 [MPa] is the pseudo-saturation pressure, as defined by Dubinin [23]. According to Eq. (3), V_a is considered constant and is also a fitted parameter.

The non-linear fitting of the curves was also carried out by considering that the density of the adsorbed phase was equal to the density of liquid hydrogen, ρ_{liq} , i.e., 70.8 kg m⁻³ at 20 K and 0.1 MPa [53]. By adopting this approach, V_a is defined as n_{abs} / ρ_{liq} . Thus, the MDA equation takes the following form:

$$\begin{aligned}
n_{exc} &= n_{max} \exp\left(\left(\frac{RT}{\alpha + \beta T}\right)^2 \ln^2\left(\frac{P_0}{P}\right)\right) - \rho_g \frac{n_{abs}}{\rho_{liq}} \\
&= \left[n_{max} \exp\left(\left(\frac{RT}{\alpha + \beta T}\right)^2 \ln^2\left(\frac{P_0}{P}\right)\right) \right] \left(1 - \frac{\rho_g}{\rho_{liq}}\right)
\end{aligned} \tag{4}$$

The pressure dependence of ρ_g was determined for each temperature considered in this study using the REFPROP-7 software and introduced into Eq. (3) and Eq. (4). The Levenberg-Marquardt algorithm was used to solve the nonlinear curve fitting in sense of least squares. All the experimental data obtained for the eleven temperatures chosen for this study were fitted simultaneously. This solution allowed obtaining a set of only five parameters valid for the entire temperature range considered.

When using the MDA equation, the isosteric heat of adsorption, Q_{st} , takes the following form:

$$Q_{st} = -\Delta H_{ads} = \alpha \sqrt{-\ln\left(\frac{n_{abs}}{n_{max}}\right)} \tag{5}$$

where n_{abs} / n_{max} is the hydrogen fractional filling of the AC pore volume, θ .

According to the second law of thermodynamics, the variation of entropy due to the hydrogen adsorption, ΔS_{ads} , and Q_{st} are related as follows:

$$\Delta S_{ads} = \frac{\Delta H_{ads}}{T} = \frac{-Q_{st}}{T} \tag{6}$$

In addition, the entropy of the adsorbed hydrogen with respect to the entropy of the perfect gas phase at 0.1 MPa and at the same temperature (ΔS_{ads}) can be calculated from the MDA equation [52]:

$$\begin{aligned}\Delta S_{ads} &= S_a - n_a s_g^0 \\ &= \frac{n_{max} \beta \sqrt{\pi}}{2} \left[1 - \text{Erf} \left(\sqrt{-\ln \left(\frac{n_{abs}}{n_{max}} \right)} \right) \right] + n_{abs} \left[\beta \sqrt{-\ln \left(\frac{n_{abs}}{n_{max}} \right)} \right] \\ &\quad + n_{abs} R \ln \left(\frac{P^0}{P_0} \right)\end{aligned}\tag{7}$$

where s_g^0 is the entropy of the perfect gas phase at 0.1 MPa and at the same temperature than the adsorbed phase, and P^0 is the reference state pressure, i.e., 0.1 MPa.

3.2 The Sips equation

The Sips equation was also used to model hydrogen adsorption on ACs. This approach allows evaluating n_{abs} as follows:

$$n_{abs} = N \frac{(aP)^k}{1 + (aP)^k}\tag{8}$$

Replacing a^k by b , Eq. (8) can be rewritten as follows:

$$n_{abs} = N \frac{bP^k}{1 + bP^k}\tag{9}$$

where N is the maximum adsorption capacity of the material, b the Langmuirian coefficient and k the coefficient related to the Freundlich equation. When k is equal to 1, equation (9) becomes the Langmuir equation. Alternatively, when P or b approaches 0, equation (9) becomes the Freundlich equation [54]. Unlike the MDA equation, the Sips equation evaluates

n_{abs} instead of n_{exc} . Thus, it is not possible to directly fit the experimental data using the Sips equation, and Eq. (2) was used to convert n_{exc} into n_{abs} . When applying the Sips equation, it was first assumed that V_a was equal to the value obtained from the fit of the data using the MDA equation, then V_a was estimated by empirical methods.

The Sips equation proved to be more appropriate than the MDA equation for studying the thermodynamics of hydrogen adsorption [55]. Indeed, the five parameters of the MDA equation do not depend on the temperature, therefore the calculated isosteric heat and the entropy of adsorption, by Eq. (5) and (7), respectively, do not depend on temperature either. The temperature dependence of the heat of adsorption can be determined by applying the Clausius-Clapeyron equation, presented in Eq. (1), to groups of three adsorption isotherms fitted using the MDA equation. Nevertheless, the MDA equation may have some limitations when evaluating the heat of adsorption because it does not take into account the formation of hydrogen clusters confined in micropores [56,57] or cooperative adsorption processes, which were observed for other gases [58,59] and may result in an increase of the heat of adsorption.

In order to evaluate the validity of both the MDA equation and the sorption isosteric method, Q_{st} was calculated using also the Sips model, taking into account the fugacity (f) instead of the pressure in all the calculations, and considering a non-constant V_a . Eq. (9) was first reformulated by considering the fugacity as a dependent variable:

$$f = \left(\frac{N}{b(N - n_{abs})} \right)^{\frac{1}{k}} \quad (10)$$

The adsorption isosteres (Van't Hoff curves) were then obtained at several fixed values of n_{abs} . Thus, Q_{st} [kJ mol⁻¹] was calculated by the linear regression applied to each adsorption isostere and on the entire range of temperature between 77 and 273 K. The following equation was used:

$$Q_{st} = -c \times R/1000 \quad (11)$$

where c is the slope of the linear regression, and R is the universal gas constant.

3.3 Specific heat at constant pressure of the adsorbed hydrogen phase

The specific heat at constant pressure of the adsorbed hydrogen phase, $c_{p,ads}$, was evaluated from Q_{st} . To do this, the Kirchhoff law applied to a physicochemical transformation was used:

$$\Delta H(T + dT) = \Delta H(T) + \int_T^{T+dT} \Delta c_p \cdot dT \quad (12)$$

In the specific case of adsorption, Eq. (12) can be written as follows [60]:

$$c_{p,ads} = c_{p,bulk} - \frac{dQ_{st}}{dT} \quad (13)$$

where $c_{p,bulk}$ [$\text{J K}^{-1} \text{mol}^{-1}$] is the specific heat at constant pressure of the hydrogen bulk phase.

The evolution of $c_{p,bulk}$ with temperature was determined by using the REFPROP-7 software.

4. Results and discussion

4.1 Textural properties of ACs

Table 1 summarises the measured textural properties of the two investigated ACs, namely MSC30 and MSP20X.

Table 1 - Textural properties of MSC30 and MSP20X.

Method	Parameter	MSC30	MSP20X
BET [47]	A_{BET} [$m^2 g^{-1}$]	3305	2363
NLDFT [21,48]	S_{NLDFT} [$m^2 g^{-1}$]	2216	2007
	S_{micro} [$m^2 g^{-1}$]	1708	1963
	S_{meso} [$m^2 g^{-1}$]	508	44
	V_{tot} [$cm^3 g^{-1}$]	1.60	0.93
	V_{micro} [$cm^3 g^{-1}$]	0.96	0.88
	V_{meso} [$cm^3 g^{-1}$]	0.64	0.05
	$V (<0.5 \text{ nm})$ [$cm^3 g^{-1}$]	0.00	0.02
	$V (0.5 - 0.7 \text{ nm})$ [$cm^3 g^{-1}$]	0.04	0.17
	$V (0.7 - 2 \text{ nm})$ [$cm^3 g^{-1}$]	0.91	0.69
Dubinin-Radushkevich and Stoeckli [61]	Average Micropore Size [nm]	1.28	1.04
Dubinin-Radushkevich [62]	V_{micro, N_2} [$cm^3 g^{-1}$]	1.02	0.83
Dubinin-Radushkevich [62]	V_{micro, CO_2} [$cm^3 g^{-1}$]	0.37	0.45

Overall, MSC30 exhibited more developed textural properties than MSP20X. First, an A_{BET} of $3305 \text{ m}^2 \text{ g}^{-1}$ was obtained for MSC30, about $700 \text{ m}^2 \text{ g}^{-1}$ more than that of MSP20X. This value confirms the limits of the BET method: in fact, the maximum possible geometrical area for a carbon material is estimated at $2630 \text{ m}^2 \text{ g}^{-1}$ [15,63]. The BET method is known to overestimate the surface area when micropores wider than 1 nm exist, since pore filling occurs instead of monolayer adsorption, which is one of the main assumptions of the BET method. To solve this problem, the specific surface area of MSC30 and MSP20X was also evaluated by using the NLDFT method, obtaining a S_{NLDFT} of $2216 \text{ m}^2 \text{ g}^{-1}$ for MSC30 and

2007 m² g⁻¹ for MSP20X. MSC30 also had a very high total pore volume, 1.60 cm³, among the highest values ever reached for an AC [25], while the measured total pore volume of MSP20X was 0.93 cm³ g⁻¹.

Figure 1 shows the PSDs calculated using the NLDFT model. MSC30 exhibited a bimodal PSD, with the first peak around 0.8-0.9 nm and the second peak around 2 nm. On the other hand, MSP20X showed a broad peak around 0.7-0.8 nm and a shoulder around 1-2 nm. Thus, the presence of supermicropores (0.7–2 nm) was observed. Furthermore, MSC30 had larger pores than MSP20X: an average micropore pore size (L_0) of 1.28 nm was found for MSC30, while a L_0 of 1.04 nm was found for MSP20X. The presence of mesopores was also observed for MSC30, whereas MSP20X was found to be an almost completely microporous carbon.

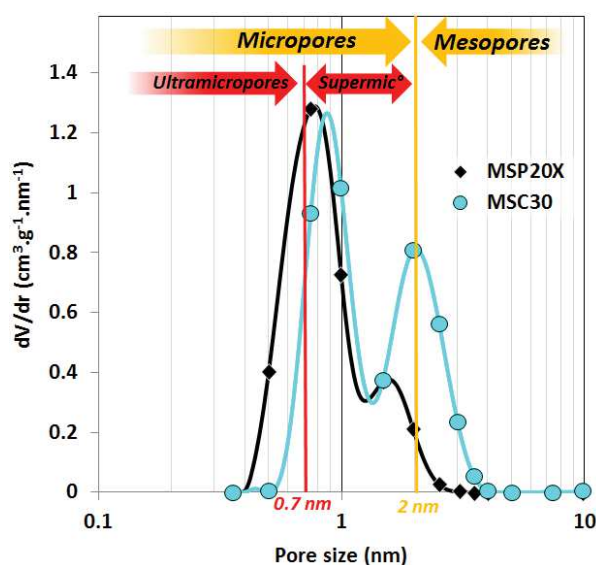


Figure 1 – PSDs of MSC30 and MSP20X (semi-log plot).

The 2D-NLDFT HS method was also used to evaluate the micropores volume (V_μ) of the two ACs. The results were compared to those obtained using the Dubinin-Radushkevich (DR) method. V_μ equal to 0.96 cm³ g⁻¹ for MSC30 and 0.88 cm³ g⁻¹ for MSP20X were obtained by 2D-NLDFT HS. The same quantities obtained using the DR equation were 1.02 cm³ g⁻¹ and 0.83 cm³ g⁻¹, respectively. Hence, 2D-NLDFT HS method gave higher values of V_μ than the

DR method applied to nitrogen isotherms because the former method also takes into account the microporosity only accessible to CO₂. Indeed, the 2D-NLDFT HS method offers several advantages over the DR method. In particular, (i) it models physisorption in slit-shaped pores; (ii) it takes into account non-uniform fluid behaviour of hydrogen confined in the pores; and (iii) it considers the adsorption of CO₂ for the evaluation of the volume of the narrowest pores in order to overcome the limitations of N₂ [64]. Thus, the higher values obtained with the 2D-NLDFT HS method can be explained by the fact that it takes better account the contribution of very narrow pores to the overall volume of micropores.

4.2 Application of the Modified Dubinin-Astakhov (MDA) equation

Figure 2 shows the excess adsorption isotherms measured for the two investigated ACs in the temperature range of 77 to 273 K and up to 15 MPa.

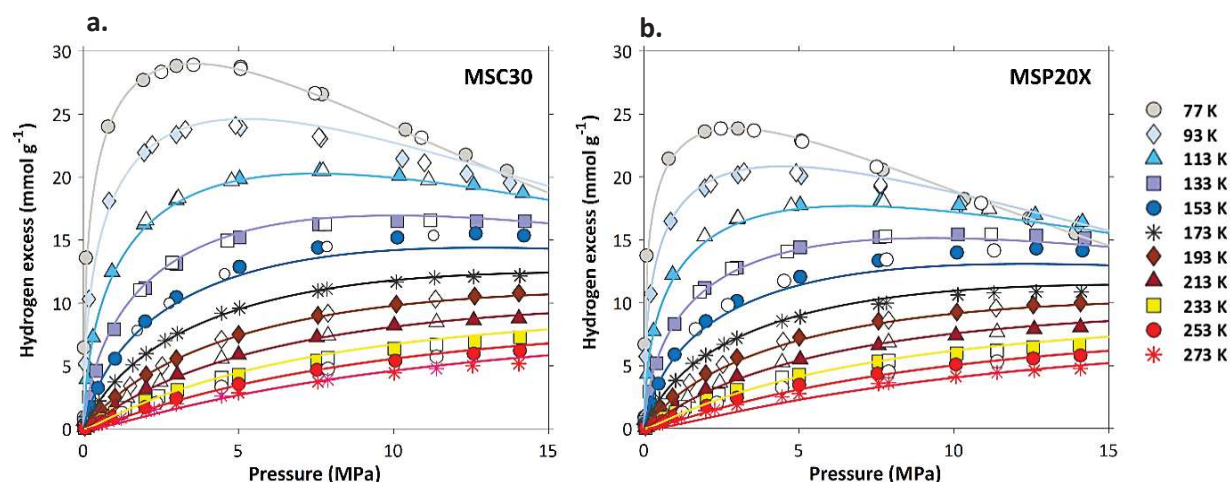


Figure 2 – Excess hydrogen adsorption-desorption isotherms of the two investigated ACs: (a) MSC30 and b) MSP20X (full and empty symbols indicate adsorption and desorption data, respectively).

The adsorption was completely reversible for all experimental temperatures investigated and the amount of hydrogen adsorbed gradually decreased by increasing the adsorption temperature. The maximum excess hydrogen uptake measured was equal to 29 mmol g⁻¹ (5.8 wt.%) and 23.8 mmol g⁻¹ (4.8 wt.%) for MSC30 and MSP20X, respectively. The higher value obtained for MSC30 over MSP20X was related to its higher specific surface area in good agreement with Chahine's rule. Figure 3a shows the correspondence between A_{BET} and the maximum excess hydrogen adsorption for the two investigated ACs and for other ACs of the open literature. Figure 3a also shows that MSP20X follows Chahine's rule perfectly, whereas MSC30 is slightly below the straight line representing the rule. Indeed, according to the Chahine rule, an A_{BET} as high as 3305 m² g⁻¹ should correspond to a higher hydrogen uptake of about 6.5 wt.%. However, this inconsistency is related to the overestimation of the specific surface area by the BET method, as mentioned previously.

By gradually increasing the temperature, the maximum hydrogen uptake decreased and progressively moved to higher pressures, which means that a maximum of adsorption is located at very high pressures for temperatures closer to 273 K. In the pressure range considered, (0-15 MPa), a maximum of the excess hydrogen adsorption was obtained only up to 153 K (Figure 3b).

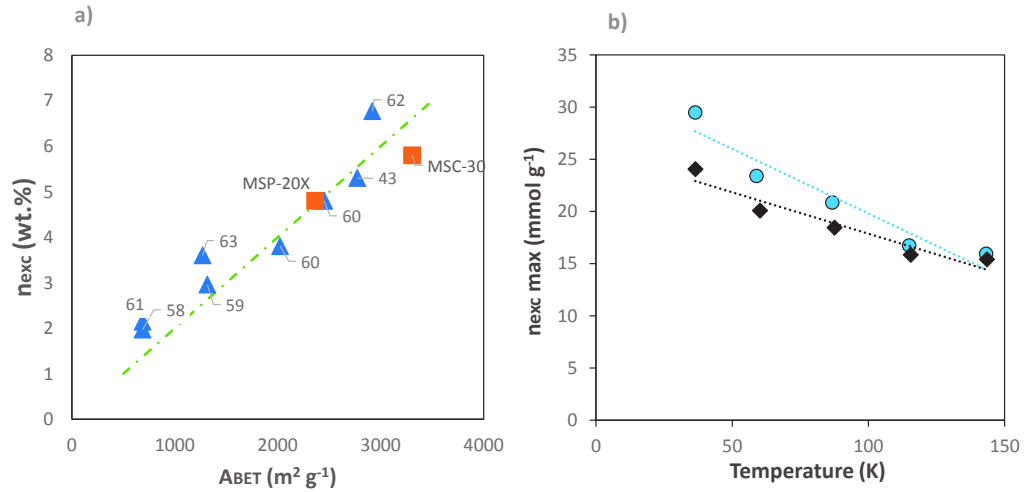


Figure 3 – a) Increase of maximum of hydrogen excess adsorption with A_{BET} and b) maximum of excess adsorption isotherms [63,65–70]

The five parameters of Eq. (3) obtained by non-linear curve fitting are listed in Table 2. The results are shown in Figure 2 with the corresponding experimental data. Overall, a coefficient of determination R^2 between 0.973 and 0.999 was obtained for each isotherm, highlighting the good quality of the fit.

Table 2 – Parameters of the Modified Dubinin-Astakhov equation obtained by non-linear fitting of adsorption isotherms for MSC30 and MSP20X, considering a constant value of V_a .

Parameter	MSC30	MSP20X
n_{max} (mol kg ⁻¹)	72.46	47.38
α (J mol ⁻¹)	3300	4094
β (J mol ⁻¹ K ⁻¹)	15.8	11.5
P_0 (MPa)	1013	632
V_a (m ³ kg ⁻¹)	0.0015	0.0011
ρ_a (kg m ⁻³)	96.6	86.93

The quality of the curve fitting remains very good even considering V_a as a variable (Figure S1 of Supplementary Information). However, the results obtained in the latter case were not as good as those obtained by considering V_a as constant. Indeed, lower coefficients of determination R^2 have been obtained and, moreover, the values of P_0 were not consistent with those found in the literature (Table S1) [46]. Figure 4 shows the evolution of V_a considering that the volume of the adsorbed phase is equal to that of liquid hydrogen. V_a was found to decrease considerably when the temperature increases. Furthermore, V_a was always lower than the values reported in Table 2 and in the pressure range considered. This could explain the high value of P_0 obtained by the curve fitting (Table S1).

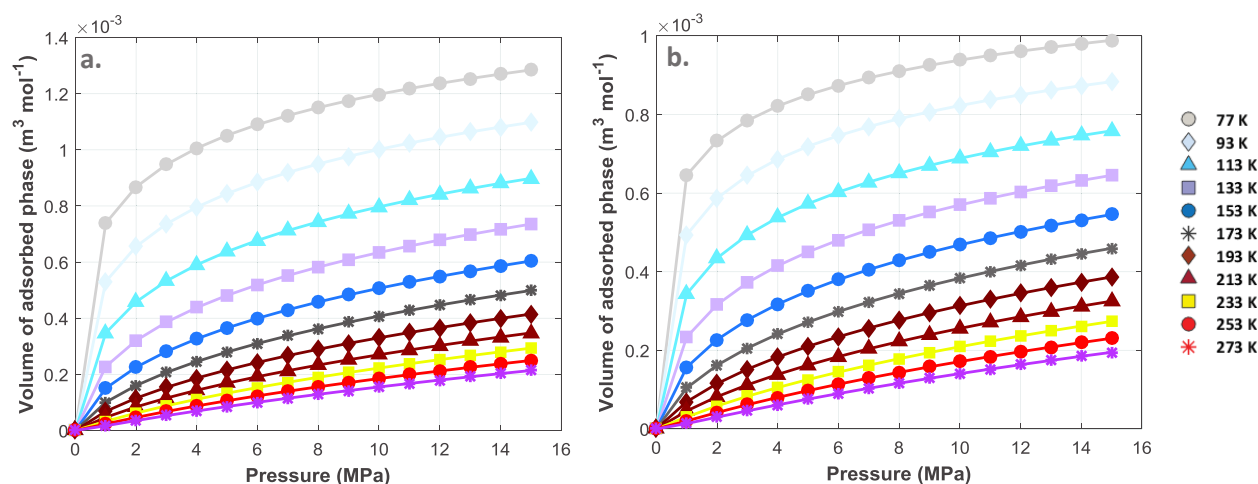


Figure 4 – Evolution of V_a as a function of pressure when one considers that the density of the adsorbed phase is equal to the density of liquid hydrogen: a) MSC30 and b) MSP20X.

Several authors have argued that the density of the adsorbed hydrogen phase can be approximated by the density of liquid hydrogen [71,72]. However, the results of our simulations have shown that hydrogen adsorption on ACs was best described by considering that V_a was constant, the density of the hydrogen adsorbed phase increasing asymptotically until reaching a stationary value when the pressure increases [73]. In one of our previous

studies, we found that the density of adsorbed hydrogen could be 66 kg m^{-3} at 77 K and 4 MPa, a little less than the density of liquid hydrogen, 70 kg m^{-3} [74]. Nevertheless, a density of adsorbed hydrogen of 96.6 kg m^{-3} was obtained for MSC30, while 87.74 kg m^{-3} was obtained for MSP20X using the parameters obtained from the fits and listed in Table 2. These values even exceed the density of solid hydrogen, i.e., 87.4 kg m^{-3} .

P_0 was found to be 1013 MPa for MSC30 and 632 MPa for MSP20X assuming that V_a was constant. Even higher values were obtained when V_a was supposed to vary (6035 MPa for MSC30 and 2217 MPa for MSP20X). P_0 represents the saturation pressure in the original model proposed by Dubinin [23], which describes gas adsorption in subcritical systems. Nevertheless, in the specific case of hydrogen adsorption, which occurs under supercritical conditions, this parameter is usually called “pseudo-saturation” pressure. Richard et al. [46] have established a relationship between the density of the adsorbed phase density and the quasi-saturation pressure, arguing that the adsorbate behaves like a supercritical fluid that should be compressed at several hundred MPa to a density equal to that of the liquid or solid form. Furthermore, Do and Do [51] have claimed that supercritical molecules can form clusters within micropores large enough to exert a quasi-saturation vapour pressure in the same way the subcritical fluids exhibit their vapour pressure. According to this theory, ACs with smaller micropores would have a lower pseudo-saturation pressure, as confirmed by our fits. We found 1013 MPa for MSC30 ($L_0 = 1.28 \text{ nm}$) and 632 MPa for MSP20X ($L_0 = 1.04 \text{ nm}$). P_0 depends on both the gas and the type of adsorbent. Richard et al. [46] found a P_0 equal to 11320 MPa for N_2 and 1850 MPa for CH_4 . In the first case, the AC C034 ($A_{BET} = 2000 \text{ m}^2 \text{ g}^{-1}$) was used, and the data fit was performed in the temperature range of 93-298 K and up to 6 MPa. On the other hand, the material CNS-201TM ($A_{BET} = 1150 \text{ m}^2 \text{ g}^{-1}$) was used for CH_4 adsorption measurements, carried out in the range of 243 to 333 K and up to 10 MPa. In the case of hydrogen, they found 1470 MPa, a value almost 30% higher than that obtained

in this study. This value was obtained using the AC AX-21 ($A_{BET} = 2800 \text{ m}^2 \text{ g}^{-1}$) up to 6 MPa. Therefore, the difference with the value of P_0 obtained by our fit can be explained both by the different textural properties and by the reduced pressure range considered. Other authors [75] found a P_0 of 322 MPa when using MOF-5TM in the case of hydrogen.

n_{max} was found to be higher for MSC30, $72.46 \text{ mol kg}^{-1}$, than for MSP20X, $47.38 \text{ mol kg}^{-1}$. This difference can be explained by the superior textural properties of MSC30 compared to MSP20X. Indeed, hydrogen adsorption on ACs is roughly proportional to their specific surface area, i.e., to their micropore volume [76,77], but it also depends on the total pore volume because the entire volume is filled at the high pressures considered in this study [20]. Thus, these values are not completely surprising if we consider the textural properties reported in Table 1.

The values of P_0 and n_{max} obtained by the isotherms fitting highlight the empirical nature of the adopted model. Indeed, according to Schlapbach and Zuttel [78], the maximum hydrogen adsorption capacity on a porous solid is $1.3 \times 10^{-5} \text{ mol m}^{-2}$, which leads to a maximum uptake of 34 mol kg^{-1} (i.e., 6.8 wt.%) for a graphene sheet whose specific surface area is $2630 \text{ m}^2 \text{ g}^{-1}$ [63]. Using the A_{BET} obtained from the textural characterisation of the two ACs studied, we calculated the hypothetical maximum hydrogen storage for both MSC30 and MSP20X, i.e., $42.96 \text{ mol kg}^{-1}$ and $30.72 \text{ mol kg}^{-1}$, respectively, which are considerably lower than the values obtained from the fit of the data (i.e., 72.46 and $47.38 \text{ mol kg}^{-1}$, respectively). In addition, the definition of V_a still remains ambiguous. Indeed, the value estimated was $1.5 \text{ cm}^3 \text{ g}^{-1}$ for MSC30, whereas V_T is $1.6 \text{ cm}^3 \text{ g}^{-1}$ for the same AC. On the other hand, the value of V_a obtained was slightly higher than that of V_T obtained by NLDFT in the case of MSP20X ($1.1 \text{ cm}^3 \text{ g}^{-1}$ against $0.93 \text{ cm}^3 \text{ g}^{-1}$). This inconsistency could be due not only to the inaccuracy in the determination of the MDA parameters, but also to the fact that V_T was obtained by fitting

the 2D-NLSDT HS model to both N₂ and CO₂ isotherms. Further experiments are underway to establish clear correlations between textural properties and MDA parameters.

4.3 Application of the Sips equation

The Sips equation was also used to model hydrogen adsorption on the two investigated ACs. Unlike the MDA equation, the Sips equation describes the evolution of n_{abs} with respect to the fugacity. Hence, Eq. (2) was used to determine n_{abs} from n_{exc} . V_a was first set to 0.0015 m³ kg⁻¹ and to 0.0011 m³ kg⁻¹ for MSC30 and MSP20X, respectively, i.e., the values obtained from the curve fitting by using the MDA equation. The fugacity of hydrogen at different temperatures and pressures was obtained using the REFPROP-7 software. Only a few isotherms have reached an asymptotic value within the defined pressure range (Figure S2 of the Supplementary Information). In addition, the difference between n_{abs} and n_{exc} was quite important at high temperature and high fugacity. For example, it exceeded 103.8 % and 102.4 % for MSC30 and MSP20X, respectively, at 273 K. This behaviour was mainly due to the disparity between fugacity and pressure (for a pressure of 14 MPa, the fugacity is 15.29 MPa). For these reasons, we concluded that the values of V_a obtained by the MDA equation do not allow an accurate evaluation of n_{abs} from experimental data.

Thus, we evaluated V_a using an empirical method. The experimental data presented in Figure 2 show that a maximum of n_{exc} was reached at 77, 93, 113 and 133 K. From the excess isotherms curves, we obtained those reaching an asymptotic value by adjusting the hydrogen fractional coverage, n_{abs} / n_{max} . In this way, we estimated V_a using Eq. (2). Figure S3, included in the Supplementary Information, shows the results obtained by applying this procedure to the adsorption isotherm at 93 K. For this particular case, V_a was found to be 0.0006 m³ kg⁻¹, which is almost 43% lower than that obtained using the MDA equation. The values of V_a related to the adsorption isotherms at higher temperatures (> 133 K), thus having no

maximum, were deduced from an exponential model obtained by fitting the values of V_a estimated for the 4 aforementioned temperatures (Figure S3). Some studies on CO₂ adsorption on ACs have reported a similar quasi-linear evolution of V_a with respect to the temperature [79].

Figure 5 shows the evolution of n_{abs} with respect to the fugacity using the Sips equation and the values of V_a calculated as described above.

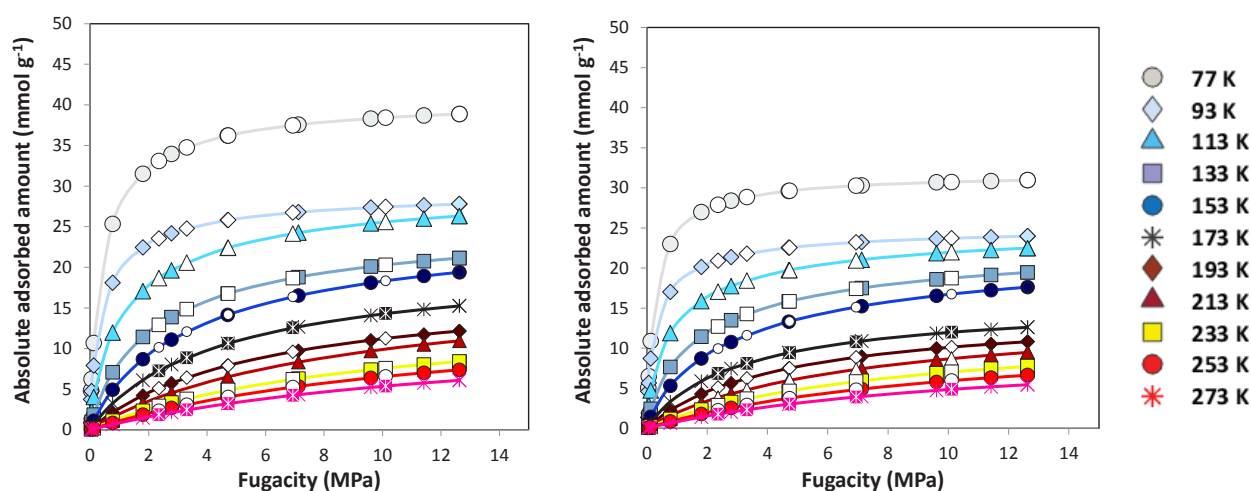


Figure 5 - Fits of the hydrogen adsorption-desorption isotherms of (a) MSC30 and (b) MSP20X with the Sips equation (full and empty symbols correspond to adsorption and desorption, respectively).

The coefficient of determination, R^2 , was higher than 0.99 for almost all isotherms. A slightly lower R^2 (~ 0.98) was obtained for the isotherm at 77 K and for MSP20X. By adopting this approach, a maximum n_{abs} equal to 37 mmol g⁻¹ was obtained for MSC30 in the pressure range considered, while an experimental maximum of 28 mmol g⁻¹ was obtained at 4 MPa (excess). These values correspond to a hydrogen adsorption equal to 7.4 wt.% and 5.6 wt.%, respectively, not too far from the upper limit for hydrogen adsorption (6.8 %) obtained experimentally by Fierro et al. [63].

Using the values of V_a estimated from the approach described above, an adsorbed hydrogen density even higher than the solid hydrogen density (86 kg m^{-3}) was obtained, especially at low temperature (Figure 6), in good agreement with some authors [80–82] who highlighted the solid-like behaviour of the hydrogen adsorbed phase. Moreover, Romanos et al. [83] found that the density of supercritical hydrogen adsorbed in nanopores could be higher than that of the condensed phase.

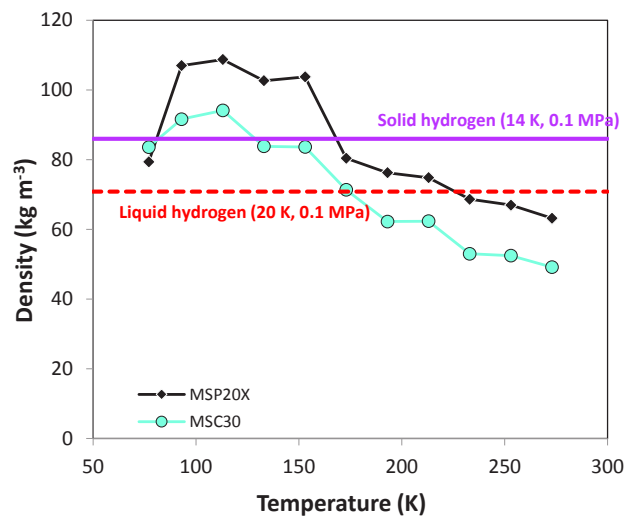


Figure 6 – Estimation of the maximum density of the hydrogen adsorbed phase as a function of temperature.

4.4 Isotheric heat of adsorption

Figure 7 shows the evolution of the isosteric heat of adsorption, Q_{st} , for various fractional fillings of the AC pore volume, θ , when using the MDA equation.

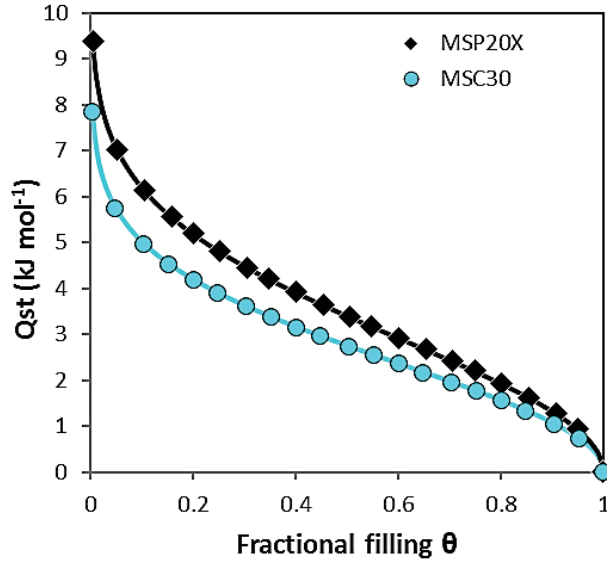


Figure 7 - Isosteric heats of adsorption obtained for hydrogen adsorbed on MSC30 and MSP20X according to the MDA equation, as a function of the fractional filling θ .

Q_{st} diverges to infinity when θ is close to zero, according to Eq. (5). Therefore, the MDA equation is not able to evaluate Q_{st} for a very small fractional filling of the AC pore volume. Nevertheless, Figure 7 shows that different stages of the adsorption process, as well as of the filling of pores, occur. Q_{st} significantly decreases in the range of $\theta \sim 0$ to $\theta = 0.2$ due to the preliminary saturation of the narrowest pores, where the adsorption forces are enhanced by the proximity of the pore walls. Thereafter, an almost linear decrease in Q_{st} is obtained because of the progressive filling of all other pores. Q_{st} decreases from 5 to 1 kJ mol⁻¹ in the θ range from 0.2 to 0.95. Finally, Q_{st} tends to zero when θ approaches 1 as the pore volume of the AC becomes almost completely saturated.

Figure 7 also shows that Q_{st} is globally higher for MSP20X than for MSC30 due to its much lower average micropore size than that of MSC30 (1.04 vs. 1.28 nm), and that narrow pores, especially ultramicropores, induce a higher Q_{st} due to the overlapping of Van der Waals forces present [12].

Figure 8 shows the evolution of the heat of adsorption calculated directly with the experimental data, thus we named it as “isoexcess”, $Q_{st,exc}$. Hydrogen was considered as an ideal gas, and the pressure was used instead of the fugacity in all calculations. In Figure 8, $Q_{st,exc}$ was reported as a function of n_{exc} , in the range 0 – 3.5 mmol g⁻¹. The evolution of $Q_{st,exc}$ in the whole range of n_{exc} can be found in Figure S5 of the Supplementary Information.

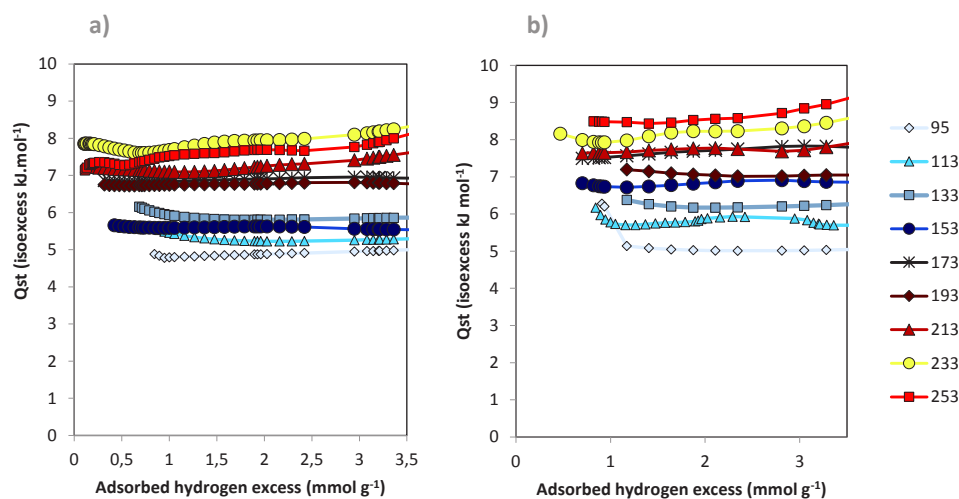


Figure 8 - Isoexcess heats of adsorption of (a) MSC30 and (b) MSP20X

$Q_{st,exc}$ values between 4.5 and 9 kJ mol⁻¹ were obtained. These values are in agreement with those obtained in our previous works [34,84], but are slightly higher than those commonly obtained for the adsorption of hydrogen on graphite [85–87]. $Q_{st,exc}$ was found to be almost constant in the range of n_{exc} considered, which corresponds to a relatively low fractional filling. Nevertheless, it increases dramatically for n_{exc} values above 3.5 mmol g⁻¹ (see Figure S5 in the Supplementary Information), which could be due in part to both the increased uncertainty and the accumulation of errors in the measurements, as concluded in previous studies [88–90]. However, lateral interactions between hydrogen molecules and cooperative adsorption could also play an important role. The increase of $Q_{st,exc}$ with θ has also been

observed for other gases, such as water [91], ethane [59], carbon dioxide [92,93] and methane [58]. Torres-Knopp et al. [94] found that lateral interactions between hydrogen molecules and cooperative adsorption lead to an increase of Q_{st} with θ .

Figure 8 also shows that the higher the adsorption temperature, the higher the $Q_{st,exc}$. The same behaviour was observed for water vapour [95], ethane [59], methane [96], n-hexane [97] and carbon dioxide [98] as well. In the case of methane [96], the increase of $Q_{st,exc}$ with temperature was explained by the increase of the specific heat capacity at constant pressure of the adsorbed phase, $c_{p,ads}$, with temperature. Furthermore, $Q_{st,exc}$ was found to increase only under supercritical conditions, while the opposite behaviour was observed under subcritical conditions. Thus, the same approach could be applied herein: the increase of $Q_{st,exc}$ with the increase of the adsorption temperature would be due to the increase of $c_{p,ads}$ with the temperature, since only supercritical hydrogen adsorption took place under the conditions of temperature and pressure investigated in the present study.

Overall, $Q_{st,exc}$ values obtained for MSP20X were higher than those found for MSC30, in full agreement with the results obtained by applying the MDA equation. Hence, we can assert that ACs with narrow pores and increased microporosity are materials providing high values of isosteric heat of adsorption (Q_{st} and $Q_{st,exc}$).

Q_{st} was then calculated by using the Sips equation (Figure 9a). It was found that Q_{st} first decreased at low n_{abs} and then it became fairly constant in the range of n_{abs} from 2 to 6 mmol g^{-1} . For relatively high values of n_{abs} (> 8 mmol g^{-1}), Q_{st} increased significantly. The linear regression performed to calculate Q_{st} was very good, a coefficient of determination $R^2 > 0.99$ was obtained for intermediate values of n_{abs} , while slightly lower values were obtained, especially for the high values of n_{abs} (Figure S7). The values of Q_{st} obtained using the Sips equation were between 5 and 7 $kJ\ mol^{-1}$, which are not too far from those obtained with the

MDA equation and the sorption isosteric method. In this case, the calculated Q_{st} was also higher for MSP20X than for MSC30, reinforcing the above conclusions.

A temperature scanning of the adsorption isosteres was also carried out to highlight the temperature dependence of Q_{st} (Figure S8 in the Supplementary Information). Figure 9a and 9b show the Q_{st} calculated in a wide range of n_{abs} for MSC30 and MSP20X, respectively.

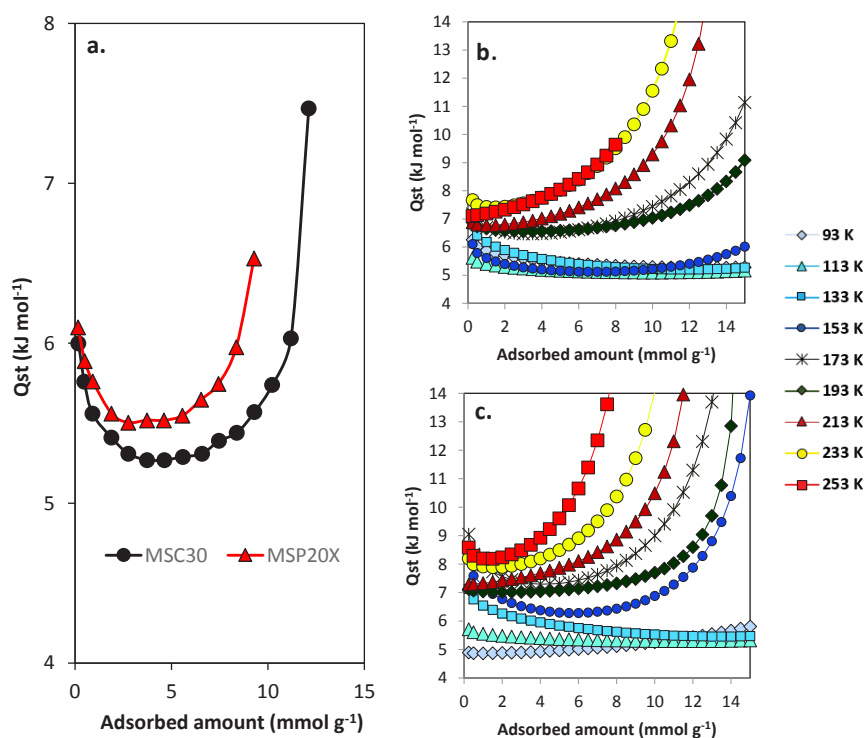


Figure 9 – (a) Temperature-averaged Q_{st} for hydrogen adsorption on MSC30 and MSP20X found using the Sips equation. Q_{st} for (b) MSC30 and (c) MSP20X, calculated by temperature scanning of the adsorption isosteres.

This additional analysis confirmed the results obtained using the Sips equation. For a specific temperature, Q_{st} initially decreased at low n_{abs} , became constant for intermediate values and increased significantly at high values of n_{abs} . In fact, the value of n_{abs} above which Q_{st} begins to diverge corresponds to the “limiting fractional filling”, θ_{lim} , which moved to lower values when the adsorption temperature increased. This behaviour could be due to a

confinement effect of hydrogen in the smallest pores. As the adsorption temperature increases, hydrogen adsorption can be particularly improved in very small pores. The temperature dependence of Q_{st} is more evident for low values of n_{abs} , as shown in Figure 11a.

Figure 10b shows the average values of Q_{st} in the temperature range between 77 and 273 K and for low values of θ (0 – 0.1) evaluated by the temperature scanning. A linear distribution was observed, just as when applying the sorption isosteric method. Moreover, Q_{st} was higher for MSP20X than for MSC30 also in this case. Thus, these results allowed to prove that the values of the isosteric heat of adsorption calculated using n_{exc} or n_{abs} are almost identical, and that the temperature dependency of Q_{st} is maintained whatever the method used. Bhatia and Myers [99] found that Q_{st} is higher at a high adsorption temperature and when using ACs with narrow pores. Their results are reported in Figure 10b with our data. The different slope of the curves can be due to both the different curvature of the carbon layers and the PSD. In fact, the ACs used in [99] exhibited different textural properties from those of MSC30 and MSP20X used in the present work, which presented an enhanced super-microporosity.

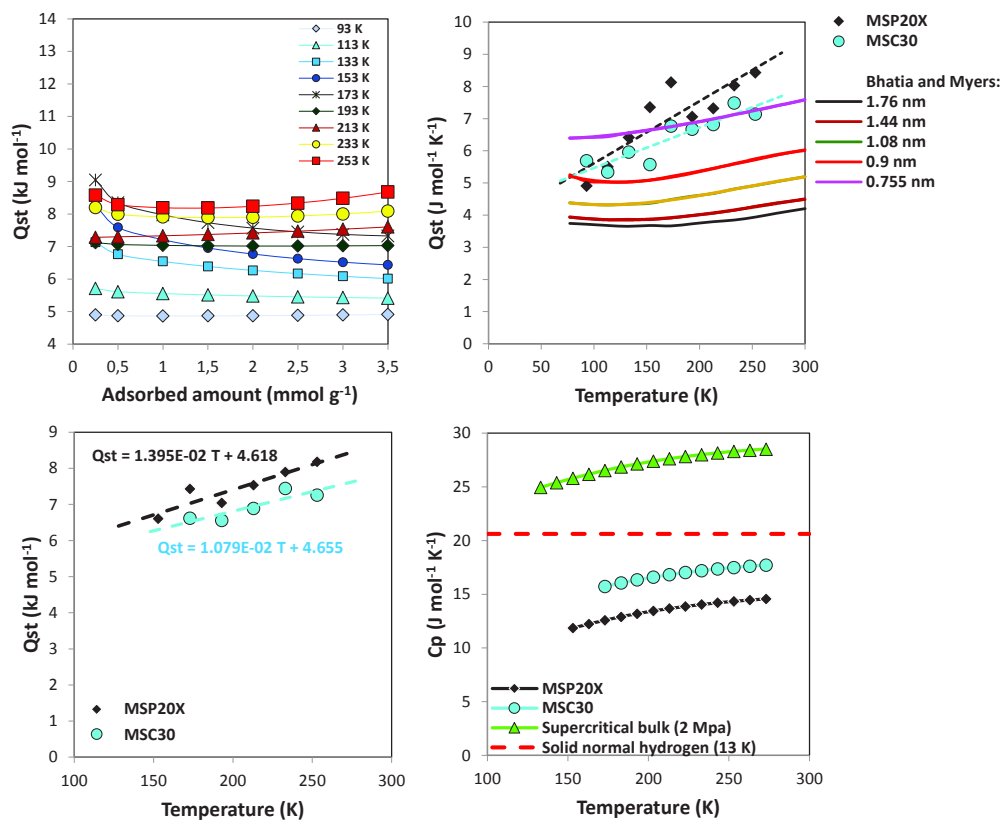


Figure 10 – Results of the temperature scanning analysis: (a) Isosteric heat of adsorption of hydrogen on MSP20X versus adsorbed amount; (b) Low-coverage average isosteric heat for MSP20X and MSC30 (with theoretical values from [99]); (c) Temperature dependence of isosteric heats of adsorption at 2 MPa; and (d) Temperature dependence of specific heat capacities of the adsorbed phase.

In conclusion, the MDA equation provided Q_{st} values between 5 and 9 kJ mol⁻¹, which are in the range of those determined by the Clausius-Clapeyron and temperature scanning methods. This range of values was slightly broader than that provided by the Sips equation, between 5 and 7 kJ mol⁻¹.

4.5 Specific heat capacity of adsorbed phase and entropy of adsorption

The specific heat capacity of the adsorbed hydrogen phase was calculated by using Eq. (12) and (13) shown in Section 3.3. The quantity dQ_{st} / dT was evaluated from the evolution of Q_{st} with respect to the temperature at constant pressure (Figure 10c). At the specific pressure of 2 MPa, this amount was found to be 10.79 and 13.95 J K⁻¹ mol⁻¹ for MSC30 and MSP20X, respectively. Figure 10d shows the evolution of $c_{p,ads}$ with temperature at a constant pressure of 2 MPa, calculated using Eq. (13). The values of $c_{p,ads}$ for MSC30 and MSP20X were both higher than those of hydrogen in solid-state and in the supercritical bulk phase. Moreover, the $c_{p,ads}$ of MSC30 was higher than that of MSP20X. $c_{p,ads}$ ranged from 10 to 18 J mol⁻¹ K⁻¹. These values are very close to those obtained in the case of methane adsorption (12 – 20 J mol⁻¹ K⁻¹), evaluated between 270 and 350 K and at 0.5 MPa [96].

The entropy of adsorption, ΔS_{ads} [kJ mol⁻¹ K⁻¹] was evaluated using the MDA equation as previously described in Section 3.1 and using Eq. (7) (Figure 11a). Absolute values of ΔS_{ads} between 0 and 9 J mol⁻¹ K⁻¹ were found by applying the MDA equation, and a linear increase with the fractional filling of the AC pore volume was obtained for both MSC30 and MSP20X. This was due to the increase of the amount of hydrogen adsorbed in the AC pore volume, resulting in an increase of Q_{st} released. Indeed, Figure 11a shows that the obtained values for ΔS_{ads} were negative, in good agreement with the exothermic nature of hydrogen adsorption.

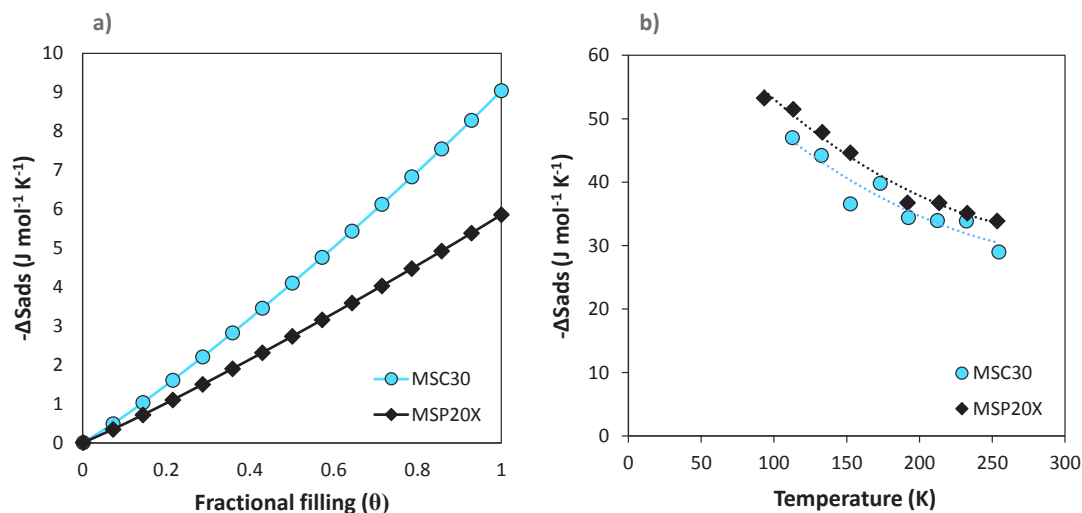


Figure 11 – (a) Entropy of hydrogen adsorption for MSC30 and MSP20X, calculated using the MDA equation; and (b) average isosteric entropy of adsorption of MSC 30 and MSP20X as a function of temperature and at low amount of adsorbed hydrogen (0-3.5 mmol g⁻¹).

Furthermore, $-\Delta S_{ads}$ was generally higher for MSC-30 than for MSP20X at any given θ , because the amount of adsorbed hydrogen at the saturation conditions, n_m , was higher, according to the values found from the fitting of the isotherms shown in Section 4.1. Increasing values of n_m lead to a more exothermic process, which explains the higher values observed for $-\Delta S_{ads}$ for MSC-30 at any given θ .

Nevertheless, the MDA equation is not able to find the temperature dependence of thermodynamic properties, as previously asserted in Section 3.2. For this reason, ΔS_{ads} was also evaluated by considering the isoexcess heat of adsorption, $Q_{st,exc}$, using Eq. (6). Figure 11b shows the average $-\Delta S_{ads}$ calculated using this additional approach, in the range of temperature 77-298 K and at low amount of adsorbed hydrogen (0-3.5 mmol g⁻¹). $-\Delta S_{ads}$ decreased when the adsorption temperature increased. This is due to the fact that $Q_{st,exc}$ does not change significantly with temperature (5 – 9 kJ mol⁻¹), whereas the ratio $Q_{st,exc} / T$ decreases when the adsorption temperature increases. $-\Delta S_{ads}$ was found to be higher for

MSP20X than for MSC-30 at any given temperature, so a higher variation in adsorption entropy was found for the AC having narrower pores (1.04 vs. 1.28 nm). Indeed, this is a consequence of the second law of thermodynamics (see. Eq. 6), since $Q_{st,exc}$ was found to be higher for AC having narrow pores (see Section 4.4). $-\Delta S_{ads}$ between 30 and 60 J mol⁻¹ K⁻¹ was obtained considering the isoexcess heat of adsorption, in the temperature range from 77 to 298 K. These values are close to those found in the literature for hydrogen adsorption on zeolites [100] and MOFs [101,102] under similar conditions.

Finally, we concluded that Q_{st} and ΔS_{ads} (in absolute values) are higher and $c_{p,ads}$ is lower, for ACs having narrow pores, as in the case of MSP20X compared to MSC30.

5. Conclusion

The Modified Dubinin-Astakhov (MDA) equation was used to investigate hydrogen adsorption on two commercial ACs with different textural properties, MSC30 and MSP20X. MSC30 had a A_{BET} higher than 3000 m² g⁻¹ and a total pore volume of 1.60 cm³ g⁻¹, whereas the A_{BET} of MSP20X was about 2363 m² g⁻¹ and the total pore volume of 0.93 cm³ g⁻¹. The superior textural properties of MSC30 led to higher hydrogen adsorption capacities (maximum of excess 5.8 wt.% at 77 K and 4 MPa, compared to 4.8 wt.% for MSP20X under the same conditions). The MDA equation proved to be a good analytical tool for understanding experimental hydrogen adsorption data over a wide range of pressures and temperatures.

In this study, the isosteric heat of hydrogen adsorption, Q_{st} , was investigated. Its dependence on both the adsorption temperature and the textural properties has been discussed. To prove the validity of the estimate obtained by using the MDA equation, Q_{st} was also calculated using the Clausius-Clapeyron and the Sips equations. The three strategies gave Q_{st} values very

close to each other, ranging from 5 to 9 kJ mol⁻¹. The higher the adsorption temperature, the higher the Q_{st} . Q_{st} was found to be higher in ACs with narrow pores and high microporosity. Finally, we calculated the heat capacity at constant pressure for the adsorbed hydrogen phase, which varied from 10 to 18 J mol⁻¹ K⁻¹; the lowest values were obtained with ACs having both narrow pores and high microporosity. The entropy of adsorbed hydrogen (in absolute values) was also found to be higher for ACs having both narrow pores and high microporosity. Further experiments are underway on more ACs to confirm these trends.

Acknowledgements

This study was partly supported by the French PIA project "Lorraine Université d'Excellence", reference ANR-15-IDEX-04-LUE, , and TALiSMAN project, funded by FEDER (2019-000214).

References

- [1] Hosseini SE, Wahid MA. Hydrogen production from renewable and sustainable energy resources: Promising green energy carrier for clean development. *Renew Sustain Energy Rev* 2016;57:850–66. doi:10.1016/j.rser.2015.12.112.
- [2] Singh S, Jain S, Ps V, Tiwari AK, Nouni MR, Pandey JK, et al. Hydrogen: A sustainable fuel for future of the transport sector. *Renew Sustain Energy Rev* 2015;51:623–33. doi:10.1016/j.rser.2015.06.040.
- [3] Marchenko OV, Solomin SV. The future energy: Hydrogen versus electricity. *Int J Hydrog Energy* 2015;40:3801–5. doi:10.1016/j.ijhydene.2015.01.132.
- [4] Ball M, Weeda M. The hydrogen economy – Vision or reality? *Int J Hydrog Energy* 2015;40:7903–19. doi:10.1016/j.ijhydene.2015.04.032.
- [5] Mazloomi K, Gomes C. Hydrogen as an energy carrier: Prospects and challenges. *Renew Sustain Energy Rev* 2012;16:3024–33. doi:10.1016/j.rser.2012.02.028.
- [6] Edwards PP, Kuznetsov VL, David WIF, Brandon NP. Hydrogen and fuel cells: Towards a sustainable energy future. *Energy Policy* 2008;36:4356–62. doi:10.1016/j.enpol.2008.09.036.
- [7] Agbossou K, Chahine R, Hamelin J, Laurencelle F, Anouar A, St-Arnaud J-M, et al. Renewable energy systems based on hydrogen for remote applications. *J Power Sources* 2001;96:168–72. doi:10.1016/S0378-7753(01)00495-5.
- [8] Edwards PP, Kuznetsov VL, David WIF. Hydrogen energy. *Philos Trans R Soc Lond Math Phys Eng Sci* 2007;365:1043–56. doi:10.1098/rsta.2006.1965.
- [9] Jain IP. Hydrogen the fuel for 21st century. *Int J Hydrog Energy* 2009;34:7368–78. doi:10.1016/j.ijhydene.2009.05.093.
- [10] Züttel A. Hydrogen storage methods. *Naturwissenschaften* 2004;91:157–72. doi:10.1007/s00114-004-0516-x.
- [11] Sircar S, Golden TC, Rao MB. Activated carbon for gas separation and storage. *Carbon* 1996;34:1–12. doi:10.1016/0008-6223(95)00128-X.
- [12] Rzepka M, Lamp P, de la Casa-Lillo MA. Physisorption of Hydrogen on Microporous Carbon and Carbon Nanotubes. *J Phys Chem B* 1998;102:10894–8. doi:10.1021/jp9829602.
- [13] Bénard P, Chahine R. Storage of hydrogen by physisorption on carbon and nanostructured materials. *Scr Mater* 2007;56:803–8. doi:10.1016/j.scriptamat.2007.01.008.
- [14] Schaefer S, Fierro V, Szczurek A, Izquierdo MT, Celzard A. Physisorption, chemisorption and spill-over contributions to hydrogen storage. *Int J Hydrog Energy* 2016;41:17442–52. doi:10.1016/j.ijhydene.2016.07.262.
- [15] Fierro V, Zhao W, Izquierdo MT, Aylon E, Celzard A. Adsorption and compression contributions to hydrogen storage in activated anthracites. *Int J Hydrog Energy* 2010;35:9038–45. doi:10.1016/j.ijhydene.2010.06.004.
- [16] de la Casa-Lillo MA, Lamari-Darkrim F, Cazorla-Amorós D, Linares-Solano A. Hydrogen Storage in Activated Carbons and Activated Carbon Fibers. *J Phys Chem B* 2002;106:10930–4. doi:10.1021/jp014543m.

- [17] Berry GD, Aceves SM. Onboard Storage Alternatives for Hydrogen Vehicles. *Energy Fuels* 1998;12:49–55. doi:10.1021/ef9700947.
- [18] Petitpas G, Bénard P, Klebanoff LE, Xiao J, Aceves S. A comparative analysis of the cryo-compression and cryo-adsorption hydrogen storage methods. *Int J Hydrog Energy* 2014;39:10564–84. doi:10.1016/j.ijhydene.2014.04.200.
- [19] Dumont E, Pré P, Le Cloirec P. Hydrogen storage by adsorption onto different activated carbons. *AIChE Annu Meet* 2006.
- [20] Fierro V, Bosch G, Siperstein FR. Pore size distribution in microporous carbons obtained from molecular modeling and density functional theory. *Stud Surf Sci Catal* 2007:519–26.
- [21] Jagiello J, Thommes M, Linares-solano A, Cazorla-amorós D, Lozano-castelló D. Characterization of Carbon Micro and Ultramicropores Using Adsorption of Hydrogen and Other Simple Gases. vol. 4. 2004.
- [22] Poirier E, Chahine R, Bose TK. Hydrogen adsorption in carbon nanostructures. *Int J Hydrog Energy* 2001;26:831–5. doi:10.1016/S0360-3199(01)00014-3.
- [23] Dubinin MM. Adsorption in micropores. *J Colloid Interface Sci* 1967;23:487–99. doi:10.1016/0021-9797(67)90195-6.
- [24] Heo Y-J, Yeon S-H, Park S-J. Defining contribution of micropore size to hydrogen physisorption behaviors: A new approach based on DFT pore volumes. *Carbon* 2019;143:288–93. doi:10.1016/j.carbon.2018.11.019.
- [25] Sdanghi G, Maranzana G, Celzard A, Fierro V. Hydrogen Adsorption on Nanotextured Carbon Materials. *Hydrog. Storage Technol.*, Wiley-Blackwell; 2018, p. 263–320. doi:10.1002/9781119460572.ch9.
- [26] Blankenship Ii TS, Balahmar N, Mokaya R. Oxygen-rich microporous carbons with exceptional hydrogen storage capacity. *Nat Commun* 2017;8:1545. doi:10.1038/s41467-017-01633-x.
- [27] Tellez-Juarez MC, Fierro V, Zhao W, Fernandez-Huerta N, Izquierdo MT, Reguera E, et al. Hydrogen storage in activated carbons produced from coals of different ranks: Effect of oxygen content. *Int J Hydrog Energy* 2014;39:4996–5002. doi:10.1016/j.ijhydene.2014.01.071.
- [28] Zhao W, Fierro V, Zlotea C, Aylon E, Izquierdo MT, Latroche M, et al. Optimization of activated carbons for hydrogen storage. *Int J Hydrog Energy* 2011;36:11746–51.
- [29] Klebanoff LE, Keller JO. 5 Years of hydrogen storage research in the U.S. DOE Metal Hydride Center of Excellence (MHCoe). *Int J Hydrog Energy* 2013;38:4533–76. doi:10.1016/j.ijhydene.2013.01.051.
- [30] DOE Technical Targets for Onboard Hydrogen Storage for Light-Duty Vehicles | Department of Energy n.d. <https://energy.gov/eere/fuelcells/doe-technical-targets-onboard-hydrogen-storage-light-duty-vehicles> (accessed February 28, 2017).
- [31] Samantaray SS, Mangisetti SR, Ramaprabhu S. Investigation of room temperature hydrogen storage in biomass derived activated carbon. *J Alloys Compd* 2019;789:800–4. doi:10.1016/j.jallcom.2019.03.110.
- [32] Zhao W, Luo L, Chen T, Li Z, Zhang Z, Wang H, et al. Synthesis and characterization of Pt-N-doped activated biocarbon composites for hydrogen storage. *Compos Part B Eng* 2019;161:464–72. doi:10.1016/j.compositesb.2018.12.122.

- [33] Zhao W, Fierro V, Fernández-Huerta N, Izquierdo MT, Celzard A. Hydrogen uptake of high surface area-activated carbons doped with nitrogen. *Int J Hydrog Energy* 2013;38:10453–60. doi:10.1016/j.ijhydene.2013.06.048.
- [34] Schaefer S, Fierro V, Izquierdo MT, Celzard A. Assessment of hydrogen storage in activated carbons produced from hydrothermally treated organic materials. *Int J Hydrog Energy* 2016;41:12146–56. doi:10.1016/j.ijhydene.2016.05.086.
- [35] Wang H, Miller DC. Thermal Management and Enhancement of Adsorption Based Onboard Hydrogen Storage System. Proceedings of the ASME 2016 10th International Conference on Energy Sustainability. June 26-30, 2016, Charlotte, North Carolina n.d.
- [36] Hermosilla-Lara G, Momen G, Marty PH, Le Neindre B, Hassouni K. Hydrogen storage by adsorption on activated carbon: Investigation of the thermal effects during the charging process. *Int J Hydrog Energy* 2007;32:1542–53. doi:10.1016/j.ijhydene.2006.10.048.
- [37] Rogacka J, Firlej L, Kuchta B. Modeling of low temperature adsorption of hydrogen in carbon nanopores. *J Mol Model* 2017;23:20. doi:10.1007/s00894-016-3202-y.
- [38] Broom DP, Webb CJ, Fanourgakis GS, Froudakis GE, Trikalitis PN, Hirscher M. Concepts for improving hydrogen storage in nanoporous materials. *Int J Hydrog Energy* 2019;44:7768–79. doi:10.1016/j.ijhydene.2019.01.224.
- [39] Kloutse AF, Zacharia R, Cossement D, Chahine R, Balderas-Xicohténcatl R, Oh H, et al. Isotheric heat of hydrogen adsorption on MOFs: comparison between adsorption calorimetry, sorption isotheric method, and analytical models. *Appl Phys A* 2015;121:2. doi:10.1007/s00339-015-9484-6.
- [40] Giraldo L, Rodríguez-Estupiñán P, Moreno-Piraján JC. Isotheric Heat: Comparative Study between Clausius–Clapeyron, CSK and Adsorption Calorimetry Methods. *Processes* 2019;7:203. doi:10.3390/pr7040203.
- [41] Lupu D, Coldea I, Misan I, Lazar M, Blanita G. Hydrogen storage potential in MIL-101 at 200 K. *Int J Hydrog Energy* 2019;44:12715–23. doi:10.1016/j.ijhydene.2018.10.099.
- [42] Fomkin AA, Pribylov AA, Murdmaa KO, Pulin AL, Shkolin AV, Men'shchikov IE, et al. Adsorption of Hydrogen in Microporous Carbon Adsorbents of Different Origin. *Prot Met Phys Chem Surf* 2019;55:413–9. doi:10.1134/S2070205119030134.
- [43] Schmitz B, Müller U, Trukhan N, Schubert M, Férey G, Hirscher M. Heat of Adsorption for Hydrogen in Microporous High-Surface-Area Materials. *ChemPhysChem* n.d.;9:2181–4. doi:10.1002/cphc.200800463.
- [44] Ma L-P, Wu Z-S, Li J, Wu E-D, Ren W-C, Cheng H-M. Hydrogen adsorption behavior of graphene above critical temperature. *Int J Hydrog Energy* 2009;34:2329–32. doi:10.1016/j.ijhydene.2008.12.079.
- [45] Tian HY, Buckley CE, Paskevicius M, Sheppard DA, Wang SB, Webb CJ, et al. Nanoscale cobalt doped carbon aerogel: microstructure and isotheric heat of hydrogen adsorption. *Int J Hydrog Energy* 2011;36:10855–60. doi:10.1016/j.ijhydene.2011.06.039.
- [46] Richard M-A, Benard P, Chahine R. Gas adsorption process in activated carbon over a wide temperature range above the critical point. Part 1: modified Dubinin-Astakhov model. *Adsorpt-J Int Adsorpt Soc* 2009;15:43–51. doi:10.1007/s10450-009-9149-x.

- [47] Rouquerol J, Llewellyn P, Rouquerol F. Is the bet equation applicable to microporous adsorbents? In: Llewellyn PL, Rodriguez-Reinoso F, Rouquerol J, Seaton N, editors. *Stud. Surf. Sci. Catal.*, vol. 160, Elsevier; 2007, p. 49–56. doi:10.1016/S0167-2991(07)80008-5.
- [48] Jagiello J, Ania C, Parra JB, Cook C. Dual gas analysis of microporous carbons using 2D-NLDFT heterogeneous surface model and combined adsorption data of N₂ and CO₂. *Carbon* 2015;91:330–7. doi:10.1016/j.carbon.2015.05.004.
- [49] Centeno TA, Stoeckli F. The assessment of surface areas in porous carbons by two model-independent techniques, the DR equation and DFT. *Carbon* 2010;48:2478–86. doi:10.1016/j.carbon.2010.03.020.
- [50] Czerny AM, Bénard P, Chahine R. Adsorption of Nitrogen on Granular Activated Carbon: Experiment and Modeling. *Langmuir* 2005;21:2871–5. doi:10.1021/la0479760.
- [51] Do DD, Do HD. Adsorption of supercritical fluids in non-porous and porous carbons: analysis of adsorbed phase volume and density. *Carbon* 2003;41:1777–91. doi:10.1016/S0008-6223(03)00152-0.
- [52] Richard M-A, Benard P, Chahine R. Gas adsorption process in activated carbon over a wide temperature range above the critical point. Part 2: conservation of mass and energy. *Adsorpt-J Int Adsorpt Soc* 2009;15:53–63. doi:10.1007/s10450-009-9150-4.
- [53] Dreisbach F, Lösch HW, Harting P. Highest Pressure Adsorption Equilibria Data: Measurement with Magnetic Suspension Balance and Analysis with a New Adsorbent/Adsorbate-Volume. *Adsorption* 2002;8:95–109. doi:10.1023/A:1020431616093.
- [54] Belhachemi M, Addoun F. Comparative adsorption isotherms and modeling of methylene blue onto activated carbons. *Appl Water Sci* 2011;1:111–7. doi:10.1007/s13201-011-0014-1.
- [55] Lam ST, Ballinger R, Forsberg C. Modeling and predicting total hydrogen adsorption in nanoporous carbon materials for advanced nuclear systems. *J Nucl Mater* 2018;511:328–40. doi:10.1016/j.jnucmat.2018.09.009.
- [56] Murata K, Kaneko K, Kanoh H, Kasuya D, Takahashi K, Kokai F, et al. Adsorption Mechanism of Supercritical Hydrogen in Internal and Interstitial Nanospaces of Single-Wall Carbon Nanohorn Assembly. *J Phys Chem B* 2002;106:11132–8. doi:10.1021/jp020583u.
- [57] Chen SG, Yang RT. Theoretical Basis for the Potential Theory Adsorption Isotherms. The Dubinin-Radushkevich and Dubinin-Astakhov Equations. *Langmuir* 1994;10:4244–9. doi:10.1021/la00023a054.
- [58] Stadie NP, Murialdo M, Ahn CC, Fultz B. Anomalous Isosteric Enthalpy of Adsorption of Methane on Zeolite-Templated Carbon. *J Am Chem Soc* 2013;135:990–3. doi:10.1021/ja311415m.
- [59] Murialdo M, Stadie NP, Ahn CC, Fultz B. Observation and Investigation of Increasing Isosteric Heat of Adsorption of Ethane on Zeolite-Templated Carbon. *J Phys Chem C* 2015;119. doi:10.1021/jp510991y.
- [60] Zhao XB, Xiao B, Fletcher AJ, Thomas KM. Hydrogen adsorption on functionalized nanoporous activated carbons. *J Phys Chem B* 2005;109:8880–8. doi:10.1021/jp050080z.

- [61] Stoeckli HF, Kraehenbuehl F, Ballerini L, De Bernardini S. Recent developments in the Dubinin equation. *Carbon* 1989;27:125–8. doi:10.1016/0008-6223(89)90165-6.
- [62] Kapoor A, Ritter JA, Yang RT. On the Dubinin-Radushkevich equation for adsorption in microporous solids in the Henry's law region. *Langmuir* 1989;5:1118–21. doi:10.1021/la00088a043.
- [63] Fierro V, Szczurek A, Zlotea C, Marêché JF, Izquierdo MT, Albiniak A, et al. Experimental evidence of an upper limit for hydrogen storage at 77 K on activated carbons. *Carbon* 2010;48:1902–11. doi:10.1016/j.carbon.2010.01.052.
- [64] Lozano-Castelló D, Cazorla-Amorós D, Linares-Solano A. Usefulness of CO₂ adsorption at 273 K for the characterization of porous carbons. *Carbon* 2004;42:1233–42. doi:10.1016/j.carbon.2004.01.037.
- [65] Md Arshad SH, Ngadi N, Aziz AA, Amin NS, Jusoh M, Wong S. Preparation of activated carbon from empty fruit bunch for hydrogen storage. *J Energy Storage* 2016;8:257–61. doi:10.1016/j.est.2016.10.001.
- [66] Sethia G, Sayari A. Activated carbon with optimum pore size distribution for hydrogen storage. *Carbon* 2016;99:289–94. doi:10.1016/j.carbon.2015.12.032.
- [67] Zhao W, Fierro V, Zlotea C, Izquierdo MT, Chevalier-César C, Latroche M, et al. Activated carbons doped with Pd nanoparticles for hydrogen storage. *Int J Hydrog Energy* 2012;37:5072–80. doi:10.1016/j.ijhydene.2011.12.058.
- [68] Li G, Li J, Tan W, Jin H, Yang H, Peng J, et al. Preparation and characterization of the hydrogen storage activated carbon from coffee shell by microwave irradiation and KOH activation. *Int Biodeterior Biodegrad* 2016;113:386–90. doi:10.1016/j.ibiod.2016.05.003.
- [69] Wang Z, Sun L, Xu F, Zhou H, Peng X, Sun D, et al. Nitrogen-doped porous carbons with high performance for hydrogen storage. *Int J Hydrog Energy* 2016;41:8489–97. doi:10.1016/j.ijhydene.2016.03.023.
- [70] Bader N, Ouederni A. Optimization of biomass-based carbon materials for hydrogen storage. *J Energy Storage* 2016;5:77–84. doi:10.1016/j.est.2015.12.009.
- [71] Kadono K, Kajiura H, Shiraishi M. Dense hydrogen adsorption on carbon subnanopores at 77 K. *Appl Phys Lett* 2003;83:3392–4. doi:10.1063/1.1621073.
- [72] Poirier E, Dailly A. On the Nature of the Adsorbed Hydrogen Phase in Microporous Metal–Organic Frameworks at Supercritical Temperatures. *Langmuir* 2009;25:12169–76. doi:10.1021/la901680p.
- [73] Dohnke E. On the high density hydrogen films adsorbed in carbon nanospaces. Thesis. University of Missouri--Columbia, 2015.
- [74] Sdanghi G, Nicolas V, Mozet K, Maranzana G, Celzard A, Fierro V. Modelling of a hydrogen thermally driven compressor based on cyclic adsorption-desorption on activated carbon. *Int J Hydrog Energy* 2019;44:16811–23. doi:10.1016/j.ijhydene.2019.04.233.
- [75] Hardy B, Corgnale C, Chahine R, Richard M-A, Garrison S, Tamburello D, et al. Modeling of adsorbent based hydrogen storage systems. *Int J Hydrog Energy* 2012;37:5691–705. doi:10.1016/j.ijhydene.2011.12.125.
- [76] Panella B, Hirscher M, Roth S. Hydrogen adsorption in different carbon nanostructures. *Carbon* 2005;43:2209–14. doi:10.1016/j.carbon.2005.03.037.

- [77] Cheng H-M, Yang Q-H, Liu C. Hydrogen storage in carbon nanotubes. *Carbon* 2001;39:1447–54. doi:10.1016/S0008-6223(00)00306-7.
- [78] Schlapbach L, Züttel A. Hydrogen-storage materials for mobile applications. *Nature* 2001;414:353.
- [79] Srinivasan K, Saha BB, Ng KC, Dutta P, Prasad M. A method for the calculation of the adsorbed phase volume and pseudo-saturation pressure from adsorption isotherm data on activated carbon. *Phys Chem Chem Phys* 2011;13:12559–70. doi:10.1039/C1CP20383E.
- [80] Jagiello J, Ansón A, Martínez MT. DFT-Based Prediction of High-Pressure H₂ Adsorption on Porous Carbons at Ambient Temperatures from Low-Pressure Adsorption Data Measured at 77 K. *J Phys Chem B* 2006;110:4531–4. doi:10.1021/jp057340x.
- [81] Silvera IF. The solid molecular hydrogens in the condensed phase: Fundamentals and static properties. *Rev Mod Phys* 1980;52:393–452. doi:10.1103/RevModPhys.52.393.
- [82] Sharpe JE, Bimbo N, Ting VP, Burrows AD, Jiang D, Mays TJ. Supercritical hydrogen adsorption in nanostructured solids with hydrogen density variation in pores. *Adsorption* 2013;19:643–52. doi:10.1007/s10450-013-9487-6.
- [83] Romanos J, Abou Dargham S, Roukos R, Pfeifer P. Local Pressure of Supercritical Adsorbed Hydrogen in Nanopores. *Mater Basel Switz* 2018;11. doi:10.3390/ma11112235.
- [84] Schaefer S, Muñiz G, Izquierdo MT, Mathieu S, Ballinas-Casarrubias ML, González-Sánchez G, et al. Rice straw-based activated carbons doped with SiC for enhanced hydrogen adsorption. *Int J Hydrog Energy* 2017;42:11534–40. doi:10.1016/j.ijhydene.2017.02.043.
- [85] Dundar E, Zacharia R, Chahine R, Bénard P. Modified potential theory for modeling supercritical gas adsorption. *Int J Hydrog Energy* 2012;37:9137–47. doi:10.1016/j.ijhydene.2012.03.021.
- [86] Kumar KV, Castro MCM de, Martinez-Escandell M, Molina-Sabio M, Rodriguez-Reinoso F. Heat of adsorption and binding affinity for hydrogen on pitch-based activated carbons. *Chem Eng J* 2011;168:972–8. doi:10.1016/j.cej.2010.12.056.
- [87] Gigras A, Bhatia SK, Anil Kumar AV, Myers AL. Feasibility of tailoring for high isosteric heat to improve effectiveness of hydrogen storage in carbons. *Carbon* 2007;45:1043–50. doi:10.1016/j.carbon.2006.12.012.
- [88] Julis J. Differential Heats of Adsorption. *Chem Zvesti* 1975;29:653–9.
- [89] Park HJ, Suh MP. Enhanced isosteric heat of H₂ adsorption by inclusion of crown ethers in a porous metal–organic framework. *Chem Commun* 2012;48:3400–2. doi:10.1039/C2CC17005A.
- [90] Bimbo N, Sharpe JE, Ting VP, Noguera-Díaz A, Mays TJ. Isosteric enthalpies for hydrogen adsorbed on nanoporous materials at high pressures. *Adsorption* 2014;20:373–84. doi:10.1007/s10450-013-9575-7.
- [91] Farmahini AH, Bhatia SK. Differences in the adsorption and diffusion behaviour of water and non-polar gases in nanoporous carbon: role of cooperative effects of pore confinement and hydrogen bonding. *Mol Simul* 2015;41:432–45. doi:10.1080/08927022.2014.976640.

- [92] Furmaniak S, Terzyk AP, Gauden PA, Harris PJF, Kowalczyk P. The influence of carbon surface oxygen groups on Dubinin–Astakhov equation parameters calculated from CO₂ adsorption isotherm. *J Phys Condens Matter* 2010;22.
- [93] Murialdo M, Ahn CC, Fultz B. A thermodynamic investigation of adsorbate-adsorbate interactions of carbon dioxide on nanostructured carbons. *AIChE J* 2018;64:1026–33. doi:10.1002/aic.15996.
- [94] Torres-Knoop A, Poursaeidesfahani A, Vlugt TJH, Dubbeldam D. Behavior of the Enthalpy of Adsorption in Nanoporous Materials Close to Saturation Conditions. *J Chem Theory Comput* 2017;13:3326–39. doi:10.1021/acs.jctc.6b01193.
- [95] Qi Shaoying, Hay K. James, Rood Mark J., Cal Mark P. Equilibrium and Heat of Adsorption for Water Vapor and Activated Carbon. *J Environ Eng* 2000;126:267–71. doi:10.1061/(ASCE)0733-9372(2000)126:3(267).
- [96] Rahman KA, Loh WS, Ng KC. Heat of Adsorption and Adsorbed Phase Specific Heat Capacity of Methane/Activated Carbon System. *Procedia Eng* 2013;56:118–25. doi:10.1016/j.proeng.2013.03.097.
- [97] Walton KS, LeVan MD. Adsorbed-Phase Heat Capacities: Thermodynamically Consistent Values Determined from Temperature-Dependent Equilibrium Models. *Ind Eng Chem Res* 2005;44:178–82. doi:10.1021/ie049394j.
- [98] Caravella A, Zito PF, Brunetti A, Barbieri G, Drioli E. Evaluation of pure-component adsorption properties of silicalite based on the Langmuir and Sips models. *AIChE J* 2015;61:3911–22. doi:10.1002/aic.14925.
- [99] Bhatia SK, Myers AL. Optimum Conditions for Adsorptive Storage. *Langmuir* 2006;22:1688–700. doi:10.1021/la0523816.
- [100] Garrone E, Bonelli B, Otero Areán C. Enthalpy–entropy correlation for hydrogen adsorption on zeolites. *Chem Phys Lett* 2008;456:68–70. doi:10.1016/j.cplett.2008.03.014.
- [101] Liu Y, Guo F, Hu J, Zhao S, Liu H, Hu Y. Entropy prediction for H₂ adsorption in metal–organic frameworks. *Phys Chem Chem Phys* 2016;18:23998–4005. doi:10.1039/C6CP04645B.
- [102] Palomino GT, Cabello CP, Areán CO. Enthalpy–Entropy Correlation for Hydrogen Adsorption on MOFs: Variable-Temperature FTIR Study of Hydrogen Adsorption on MIL-100(Cr) and MIL-101(Cr). *Eur J Inorg Chem* 2011;2011:1703–8. doi:10.1002/ejic.201001116.